SCALING ANALYSIS OF AN IBLOCA COUNTERPART TEST BETWEEN THE ATLAS AND LSTF FACILITIES

M. Lorduy-Alós, S. Gallardo and G. Verdú

Instituto Universitario de Seguridad Industrial, Radiofísica y Medioambiental

Universitat Politècnica de València, València, Spain.

Abstract:

The experiments carried out in test facilities improve knowledge of the phenomena that would occur in a nuclear power plant during an accident, and support the validation of the thermal-hydraulic codes used in the nuclear safety analysis. Among them, counterpart tests between two facilities allow analyzing the different technology and scale effects, and the inherent distortion, in the evolution of a specific transient. Thus, counterparts contribute to address the scaling methodologies and enhance confidence in extrapolating results from the facilities to their reference power plants.

The objective of this study is to analyze an Intermediate Break Loss-Of-Coolant Accident (IBLOCA) counterpart test at the ATLAS and LSTF facilities. The experiment is based on a 13% break in a cold leg, followed by the actuation of the High Pressure Injection (HPI), accumulators and Low Pressure Injection (LPI) systems. The study is supported by the simulation of the experiment with the TRACE5 thermal-hydraulic code. The results are compared with the available data of the A5.2 and IB-CL-05 tests, in the OECD-ATLAS and OECD/NEA ROSA-2 projects, respectively, in order to evaluate the prediction capabilities of TRACE5 and clarify the causes of the important differences between the transients. The analysis is completed by calculating the dimensionless π-monomial groups derived from the first approach in the top-down scaling. The comparison of the groups determines, since an analytic point of view, the relevant phenomenology during the transient and the scaling distortion between both facilities. The system scaling analysis assesses a great similarity in the evolution of the main thermal-hydraulic parameters and in the operation of the safety systems throughout this transient.

1. INTRODUCTION

Test facilities are intended to reproduce the behavior of their reference power plants. There, several experiments are carried out to generate data series with which achieve a deeper knowledge of the phenomena that would occur during an accident and to validate the thermal-hydraulic codes used in the nuclear safety analysis. Among various types of experiments, counterpart tests between two facilities constitute a significant means to address the scaling methodology and enhance confidence in extrapolating results from the facilities to their reference power plants. These tests allow analyzing the different technology and scale effects, and the inherent distortion, in the evolution of the same transient. To that end, the tests are designed so that a set of initial and boundary conditions are preserved, i.e., thermal-hydraulic state (temperature, pressure and flow condition), heat and mass sources or sinks (scaled core power or break size) and the characteristics and actuation set-points of the safety systems. Regarding the use of the codes in the nuclear safety analysis, the reliability of the models of the power plants must be verified. Given a proper model of the facilities, the codes can simulate correctly certain phenomena;

however, this capability does not ensure that the level of accuracy in a different scale or in a plant model is maintained. For this reason, it is important to test the codes response with other similar facilities ([1]Freixa et al., 2013).

In this framework, several authors have released their studies about scaling issues in counterpart tests. [2]Belaid et al. (2010) question the use of the Core Exit Temperature (CET) as a valid criterion to predict the Peak Cladding Temperature (PCT) since significant difference between both temperatures was observed in test facilities and also the correlation CET-PCT differs among the facilities. [3]Lafi and Reyes (2000) compare a station blackout sequence and show that the timing of the key events is maintained between the Reduced-Height Reduced-Pressure facility APEX and the Full-Height Full-Pressure facility LSTF. [4]Park et al. (2014) present the SBLOCA transient results in two different small-scale integral test facilities, VISTA and FESTA, which were used for the design and licensing of the SMART reactor. The counterpart test allowed identifying all the thermal-hydraulic phenomena that are expected to occur during a small break loss of coolant accident (SBLOCA) accidents. [5]Carlos et al. (2016) study and simulate with TRACE5 code the accidental sequence that follows an SBLOCA equivalent to 1.5% of the hot leg in the LSTF and PKL facilities. By modifying some features of the vessel models, the importance of the facility design in the evolution of the transient was evidenced. [6]Park et al. (2017) perform a 1% SBLOCA counterpart test in ATLAS whose target scenario is an equivalent experiment in the LSTF facility. In addition to investigating the effects of AM actions on the core heat-up and loop seal clearing phenomena, this test was purposed with the main objective of addressing scaling issues between the test facilities. Besides, [7]Yang et al. (2013) reproduce the International Standard Problem (ISP)-42 with models of the PANDA and PUMA facilities to address the scaling methodology on the response of passive safety systems. As a result of this work, some functions of the systems were confirmed in agreement with qualitative similarities, such as the Passive Containment Safety System (PCSS) start-up and normal operation, and the discharge of the Gravity-Driving Cooling System (GDCS).

The Loss of Coolant Accidents (LOCA) are discussed in the risk assessment of Light Water Reactors (LWR). The type, location, and frequency of the break of this design basis event are proved to be dependent on the size of the pipes and, as a consequence, also the thermal-hydraulic responses differ among the scenarios. Thus, in the full spectrum of sizes of a LOCA, a double-ended guillotine break of a large main pipe is less likely to occur than a rupture in a smaller pipe ([8]Takeda et al., 2012). Small Break and Large Break LOCAs (SBLOCA and LBLOCA) are extensively analyzed by means of experiments in the integral test facilities, however, data about intermediate breaks (IBLOCA) have been very limited despite these scenarios can differ significantly from the other types of break. Moreover, the IBLOCA analysis has become necessary to evaluate the core integrity during the accidents, e.g. to define correlations between the highest PCT and the break area ([9]D'Auria, 2017). In view of this, the USNRC proposed in 2005 the intermediate break as a design basis event for the assessment of the effectiveness of emergency core cooling systems ([10]USNRC, 1998). Since that time, some experiments related to the effects of these breaks have been conducted and studied to enhance the understanding of the characteristic phenomena, and also to improve the operating efficiency of the new reactor designs ([11]Bajorek and Petkov, 2001). [12]Addabbo and Annunziato (2012) summarize the major achievements of the extensive research program in LOBI, among which highlights the identification of relevant thermal-hydraulic phenomena in an IBLOCA. [13]D'Auria et al. (2000) conclude the possibility of using some facilities designed for the reproduction of SBLOCAs, such as SPES, to simulate IBLOCA transients. [14]Abe et al. (2014) analyze the capabilities of the RELAP5 code to simulate the two intermediate breaks (13% and 17%) in LSTF belonging to the OECD/NEA ROSA-2 Project. The wide experimental program of beyond-design-basis accidents (BDBA) performed by the Korea Atomic Energy Research Institute (KAERI) in ATLAS facility comprises the investigation of IBLOCA scenarios, including risk-informed break size definitions ([15]NEA, 2016). ATLAS experiments were conceived with a double function. On one side, to increase the availability of data referring to IBLOCA accidents. On the other side, the tests are equivalent to those of LSTF, so they are feasible to perform counterpart tests ([16]Bestion et al., 2017).

This work compares the 13% IBLOCA experiments carried out in Advanced Thermal-Hydraulic Test Loop for Accident Simulation (ATLAS) and in Large Scale Test Facility (LSTF). To that end, two models of the facilities are used to reproduce the tests with TRACE5 thermal-hydraulic code. First, the similarities and differences of the results between both facilities are analyzed attending the importance of

thermal-hydraulic phenomena in the ranking table PIRT for IBLOCA built by [17]Takeda and Ohtsu (2017). The use of the simulation code makes possible to obtain thermal-hydraulic parameters that are difficult to measure in a facility. Thus, the analysis is completed since an analytic point of view by calculating the dimensionless scaling groups that characterize the phenomenology.

The paper is organized as follows: Section 2 presents a brief description of ATLAS and LSTF facilities, their TRACE5 models and the global system scaling methodology applied in a subsequent section. The 13% IBLOCA test procedure and the simulation results are provided in Section 3. In Section 4, the first approach of the top-down scaling methodology, the global system response, is applied to quantify the scalability and distortion of the transient between both facilities.

Nomenclature

A	area
d_h	hydraulic diameter
h	enthalpy
H	total height
j	flux
l	length
L	liquid height
$\dot{m}$	mass flow rate
M	total mass
p	pressure
$\dot{q}$	heat transfer
t	time
T	temperature
V	control volume
Δ	difference
Ψ	property
μ	specific internal energy
Π_x	π-monomial of a magnitude x
ρ	density
τ	residence time
υ	specific volume
ω	transfer characteristic frequency
$\Xi_{x,y}$	π-monomial group of a property x that changes due to a property y

Subscripts

0	reference
g	gas phase
in	inlet
l	liquid phase
m	two-phase mixture
out	outlet
sat	saturation conditions

Acronyms

ACC	Accumulator
AM	Accident Management
CCFL	Counter Current Flow Limit
CET	Core Exit Temperature
DBA	Design Basis Accident
DEGB	Double-Ended Guillotine Break
ECCS	Emergency Core Cooling System
HPI	High Pressure Injection
IBLOCA	Intermediate Break LOCA
JAEA	Japan
KAERI	Korea Atomic Energy Research Institute
LBLOCA	Large Break LOCA
LOCA	Loss Of Coolant Accident
LPI	Low Pressure Injection
LSTF	Large Scale Test Facility
LWR	Light Water Reactor
MSLB	Main Steam Line Break
PCT	Peak Cladding Temperature
PIRT	Phenomena Identification Ranking Table
PWR	Pressurized Water Reactor
ROSA	Rig Of Safety Assessment program
RPV	Reactor Pressure Vessel
SBLOCA	Small Break LOCA
USNRC	U.S. Nuclear Regulatory Commission
TRACE	TRAC/RELAP Advanced Computational Engine

2. METHODOLOGY

2.1 ATLAS and LSTF facilities

ATLAS is an integral effect test facility destined to recreate the major Design Basis Accidents (DBAs) in its reference reactor, the APR1400 ([18]KAERI, 2014), including breaks in all types of lines, e.g. hot and cold legs, Direct Vessel Injection (DVI) line and Main Steam Line. The design is based on the three-level scaling methodology of Ishii and Kataoka to preserve the transient response of major variables and to enhance the reproduction of the loop-asymmetric phenomena ([19]Choi et al., 2017). In addition, the design maintains the Reduced-height Full-pressure criterion, being its geometrical scaling ratios ½ height, 1/144 area and 1/288 volume. Hence, characteristic values for the pressure or temperature are preserved but, due to the height reduction, the thermal-hydraulic phenomena occur $\sqrt{2}$ faster than expected in the APR1400 and the duration of the tests is shortened.

The facility includes different features of Generation IV nuclear reactors distributed along a primary system, secondary system, safety system, break system and an auxiliary system. The primary system comprises a vessel (RPV) surrounded by an annular downcomer, a pressurizer and two loops composed of a hot leg, a steam generator tube bundle, two intermediate and cold legs and two pumps, each one. The fuel rod assemblies in the reference PWR are simulated by means of 396 electrical heater rods with the capability to supply 2.15 MW (11% of the scaled power). The secondary system consists of two steam generators, their steam lines and one condensation and refrigeration loop.

The LSTF represents a four-loop Westinghouse type reactor of 3423 MW ([20]JAEA, 2003), like that in Tsuruga Unit-2 of the Japan Atomic Power Company. The facility is built by following a Full-height Full-pressure design and its components are scaled 1/1 in height and 1/48 in areas and volumes, except the hot and cold legs. Since the four primary loops of the reference plant are lumped into two equal volume loops, these pipes are defined by a scaling factor of 1/24 in area to conserve the volumetric scale and the relation of the length to the diameter square-root ($L/\sqrt{D}$) ([21]Nakamura et al., 2009). The facility consists of a pressure vessel, a pressurizer, two symmetric primary loops, full Emergency Core Cooling System (ECCS) and two steam generators. Each loop includes a hot leg, a tube bundle consisting of 141 full-size U-tubes, a coolant pump, a loop seal and a hot leg. The core power is generated by means of 1008 heated rods able to supply 10 MW (14% of the reference scaled power). The secondary system comprises two steam generators and their main and auxiliary feedwater pumps.

2.2 TRACE5 models of ATLAS and LSTF

The facility models have been built using the TRACE5 thermal-hydraulic code, developed by the United States Nuclear Regulatory Commission ([22]USNRC, 2010). The loops, U-tube bundles, injection lines, accumulators and other ducts consist of PIPE components. The reactor pressure vessels are modeled with a 3D-VESSEL component to allow the simulation of multi-dimensional phenomena. The Pilot Operated Safety Relief Valve (POSRV) at the top of the pressurizer and the safety valves and relief valves at the steam generators are VALVE components. The reactor coolant pumps are implemented with PUMP components, for which the performance curves (head and torque) are programmed. The core power is supplied by POWER components that transfer the power to the respective rod assemblies modeled with cylindrical HEAT STRUCTURE components (HTSTR). Moreover, HTSTRs replicate the heat transfer through the tube bundles in the steam generators and the heat losses to the environment. It is demonstrated that the heat losses in test facilities are decisive on natural circulation phenomena. Thus, modeling techniques based on the results of separate effect tests and simulations ([23]Lorduy-Alós et al. 2018) are used to size de HTSTRs and select the convective heat transfer coefficients that act as a boundary condition.

During an IBLOCA, countercurrent flow limitation (CCFL) phenomenon is expected to occur in sections where high energetic steam flow, such as that produced during the boil-off, coexists with coolant flowing in the opposite direction ([24]Freixa et al., 2017). Concretely, CCFL may appear at the upper core plate, along the hot legs and at the U-tubes inlet. In ATLAS facility, it also occurs at the perforated upper plenum plate. CCFL TRACE5 option has been set up at the mentioned locations by making use of the Wallis correlation and the coefficients suggested in NUREG_IA-0203 ([25]Kim and No, 2001).

Efforts have been focused on the modeling of the break boundary conditions to simulate properly the discharged inventory and the primary system depressurization during the transient. The discharge lines have not been explicitly modeled. Instead, the break units are simplified into a PIPE, which is jointed upwardly to the cold leg throw a cross-flow junction, a VALVE and a BREAK component. Besides, TRACE offtake model and the choked-flow models (Burnell model for liquid critical flow and Ransom and Trapp model for two-phase critical flow) are set on the break nozzle to simulate a discharged flow coherent to experimental data ([26]Oussoren et al., 2017).

Figure 1 shows the nodalization sketches of the ATLAS and LSTF models using the Symbolic Nuclear Analysis Package software (SNAP).

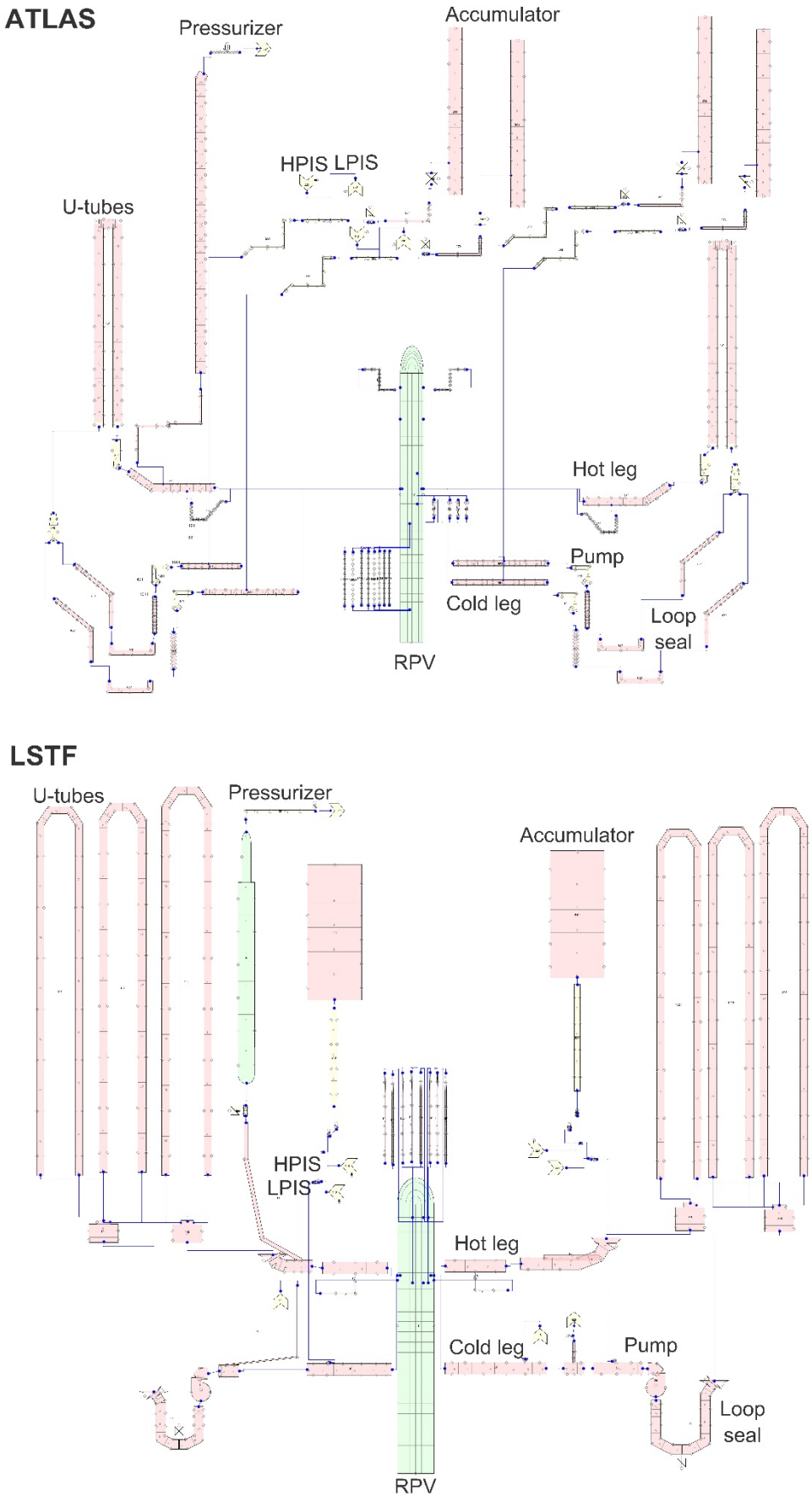

Figure 1: Nodalization of ATLAS and LSTF.

2.3 Global system scaling analysis

In this work, a scaling analysis is developed to assess the capability of ATLAS and LSTF to reproduce the overall system behavior of each other and to extend that the global processes and phenomena taking place during a 13% IBLOCA in a cold leg will occur in both facilities.

The methodology used is the dimensionless analysis carried out in the first approach, the top-down scaling, of some of the relevant scaling methodologies (Hierarchical Two-Tired Scaling (H2TS) ([27]Zuber, 1991), Fractional Scaling Analysis (FSA) ([28]Zuber et al., 2007), Three Level Scaling ([29]Ishii and Kataoka, 1983) ([30]Ishii et al., 1998). In the top-down scaling, the criteria of the global system response and the system interactions are established to relate a reduced test facility and its reference reactor. It also allows ranking the phenomena classified as important in the PIRT exercises (Phenomena Identification Ranking Table) and identifies scaling distortions.

The dimensionless analysis aims to understand a physical phenomenon by reducing the number of variables involved in it to a number of monomials without dimensions that describe the phenomenon with the same precision as the initial approach, only with fewer variables ([31]Buckingham, 1914). Moreover, if it has been established that a law between dimensional variables is equivalent to one between dimensionless variables, the second law is also fulfilled at other scales. This enables using the dimensionless analysis to compare ATLAS and LSTF behaviors. In order to perform the analysis of a hydraulic transient, the first step consists in its division into time intervals, or phases, based on their respective governing phenomena. Each phase can be described by the three conservation equations (mass, energy and momentum), for which the whole facilities are simplified into control systems. In the mass and energy equations, the system is a control volume and for the momentum equation, the control system is a loop. Next, the conservation equations are combined with caloric equations of state and thermodynamic relations to form the model that governs the significant processes, e.g. a pressure rate equation ([32]Barenjee, 1997) ([33]Muñoz-Cobo et al., 2018). The new equations can be expressed in dimensionless form by defining and substituting dimensionless parameters in terms of the constant initial and boundary conditions. Then, the yielded non-dimensional groups, also called π-monomial groups, $\Xi x,y$, from the normalized equations indicate the relative importance of a parameter y in the changes of a parameter x. That is, if the phenomenon at issue, $\dot{x}$, involves several transfer processes ($\Xi\dot{x},y_1$, $\Xi\dot{x},y_2$, …, $\Xi\dot{x},y_n$), the π-groups can be compared to that whose value is equal to 1.

The numerical value of the dimensionless groups is used to rank the transfer processes and establish the hierarchy of their importance. Hence, a process is considered important if the associated π-monomial group is greater than 1/10 of the largest π- group ([34]Wulff and Rohatgi, 1998).

The criterion to evaluate the distortion in the scaling analysis relates the π-monomial groups of two facilities. Since the groups are derived from fixed geometrical parameters and operating variables at reference conditions, they are constant and there is only one group for each transfer process. Hence, the ratio between the groups of both systems representing the same phenomenon indicates the degree of correlation or distortion. In respect of this ratio, a value close to 1 indicates similarity. For this criterion [35]Wulff (1996) establishes three regions to classify the distortion:

Phenomenon well scaled $\frac{1}{2} < \frac{\Xi x,y\ Facility}{\Xi x,y\ Prototype} < 2$

Noticeable scaling distortion $\frac{1}{3} < \frac{\Xi x,y\ Facility}{\Xi x,y\ Prototype} < \frac{1}{2}$ or $2 < \frac{\Xi x,y\ Facility}{\Xi x,y\ Prototype} < 3$

Significant scaling distortion $\frac{\Xi x,y\ Facility}{\Xi x,y\ Prototype} < \frac{1}{3}$ or $\frac{\Xi x,y\ Facility}{\Xi x,y\ Prototype} > 3$

If the π-groups have a different sign, the ratio $\frac{\Xi x,y\ Facility}{\Xi x,y\ Prototype}$ is lower than 0 and the phenomenon is completely distorted.

This scaling approach has usually been used to evaluate the relevance of the phenomena and the scaling distortion over a single transient in a test facility and its reference power plant. Ishii and Kataoka developed a scaling analysis for a natural circulation loop under single-phase and two-phase flow conditions ([29]Ishii and Kataoka, 1983) that laid the foundations for the H2TS methodology by using a LOFT facility model and a typical loop in a LWR model. [34]Wulff and Rohatgi (1998) analyzed the scaling effects between an AP600 reactor and three test facilities (APEX, LSTF and SPES) during a 1-inch Cold-Leg break. Furthermore, [36]Liao (2016) and [33]Muñoz-Cobo et al. (2018) presented the application of this scaling analysis between a test facility, LSTF, and a Westinghouse 3-loop PWR for two different SBLOCA transients.

Concerning the present IBLOCA analysis, the methodology is applied at the primary system level to four phases: blowdown, natural circulation, high quality discharge and refilling. The conservation equations are combined with caloric equations of state and thermodynamic relations to form the model that governs the depressurization and discharge processes.

The main goal of applying this methodology is to evaluate the scalability of phenomena and quantify their distortion through an analytical study. The objectivity of this method enhances confidence counterpart tests as a technique to promote the understanding of accident phenomena and address the scaling issue. Moreover, the advantage of using TRACE5 in a scaling analysis lies in being able to obtain any thermal-hydraulic parameter required in the calculation process, beyond the geometrical parameters of the facilities or the thermal-hydraulic magnitudes measured during the experiments.

3. 13% IBLOCA EXPERIMENT

3.1 Test description

The test considered in this work is a 13% cold leg IBLOCA in ATLAS (Test A5.2 in OECD-ATLAS Project) ([37]Bae, 2017). It is based on an IBLOCA in the LSTF (Test 7 in OECD/NEA ROSA-2 project, IB-CL-05) ([38]JAEA, 2013), conducted on June 14, 2012. From these test boundary conditions and the facilities scaling ratios, the test A5.2 conditions were established to carry out, in 2016, the relevant experiment to perform a counterpart test.

The primary objective of the experiment is to provide insight into the pressurized reactors response during an IBLOCA. In particular, the accident is due to the Double-Ended Guillotine Break (DEGB) of one of the Emergency Core Cooling System (ECCS) piping nozzle connected to a cold leg. An upwardly mounted long break nozzle on the cold leg reproduces this type of accident. Under these conditions, full injection of the ECCS and total failure of auxiliary feedwater were assumed as the management accident measures.

In this transient, the break produces the loss of a large quantity of coolant. Then, the safety systems are activated successively and based on the primary system pressure, to lead the facilities to stable conditions. To this end, the High-Pressure Injection (HPI) system, the accumulators and the Low-Pressure Injection (LPI) system compensate, only from the loop with pressure, the lost inventory. Table I shows the main events during the transient and the signals which cause them.

Table I. Sequence of events and control logic.

Event	Signal
Start of test - Break	T=0 s
SCRAM signal	Primary pressure < P_{SCRAM}
Coastdown of pumps	SCRAM
Power decay	SCRAM
Feedwater termination	SCRAM
MSIV closure	SCRAM
HPI initiation	Primary pressure < P_{HPI}
Accumulators injection	Primary pressure < P_{ACC}
LPI initiation	Primary pressure < P_{LPI}

The initial and boundary conditions in the ATLAS test were established from the conditions in the IB-CL-05 test and the scaling ratios between ATLAS and LSTF. For being the facilities Full-pressure scaled, both the temperature and pressure are the same in the tests. Table II presents the scale ratios used to establish the initial test conditions in ATLAS from the LSTF parameters. To achieve the initial steady-state conditions, the core power had to be modified to be 57 % of the ideally scaled power.

Table II. Scale ratios between ATLAS and LSTF parameters.

Parameter	Scale ratio ATLAS/LSTF
Power	$l_0^{1/2} d_0^{2} = 0.28$ (modified 57% ideal)
Pressure in the pressurizer	P = 1
Liquid level in the pressurizer	$l_0 = 0.52$
Core inlet temperature	T = 1
Core outlet temperature	T = 1
Mass flow through the core	$l_0^{1/2} d_0^{2} = 0.28$ (modified 56% ideal)
Break area	$l_0^{1/2} d_0^{2} = 0.28$
Secondary pressure	P = 1
Liquid level in steam generators	$l_0 = 0.52$
Feedwater mass flow rate	$l_0^{1/2} d_0^{2} = 0.28$ (modified 56% ideal)

3.2 Simulation results

This section presents the qualitative analysis of the tests A5.2 and IB-CL-05 in ATLAS and LSTF, respectively. The following, the experimental results are shown together with their simulation as normalized values (NV), which correspond to the value at every moment divided by a representative value of each parameter in the ATLAS facility. Pressures are normalized respect its initial value and the PCTs, accumulated mass flows to the break and the mass flows injected by the ECCS respect their maximum values. The time axis is normalized to the test A5.2 duration. To compare the evolution of both experiments, the LSTF results are also scaled according to the ratios presented in the previous section. Due to the ratio of height l_0=½ between the facilities, a single event occurs in LSTF slower than in ATLAS. Hence, the ratio $l_0^{1/2}$=0.72 is applied to the time scale of LSTF.

Table III summarizes the chronology of major events during the transients. It highlights the simultaneity of the simulated and experimental actuation of the safety systems in ATLAS. The only notable discrepancy is the advance in the LPI system injection. Moreover, all the events happen practically at the same time in ATLAS and LSTF simulations.

Table III: Time of occurrence of the main events

Event	Time after break		
	ATLAS Test A5.2	TRACE5 ATLAS	TRACE5 LSTF (scaled)
Break	0	0	0
SCRAM signal	0.006	0.005	0.007 (0.005)
HPI injection	0.03	0.02	0.04 (0.03)
PCT excursion	0.06	0.06	0.09 (0.07)
Start of ACC discharge	0.16	0.16	0.20 (0.15)
End of ACC discharge	0.33	0.34	0.61 (0.44)
LPI injection	0.68	0.57	0.83 (0.6)
End of test	1	1	1.5 (1.08)

The test starts by opening the break valve. The high pressure and temperature conditions cause a large loss of liquid for a short period and the rapid decrease in pressure triggers a SCRAM signal. From the SCRAM on (P_{SCRAM}), the core power follows a programmed decay heat curve, the main steam isolation valves (MSIV) and main feedwater lines are closed and the reactor coolant pumps remain stopped. Due to the secondary side isolation, the pressure in the steam generators increases up to the main steam safety valves (MSSV) set point and then it is regulated by cyclic openings.

Figure 2 shows the accumulated inventory released through the break. In the beginning, the experimental results for the discharged flow are in a very good agreement with the simulated ones for reproducing the loss of coolant. When stratification appears in the broken cold legs and the flow condition at the break changes to two-phase flow and one-phase gas, there is a slight overestimation of the mass flow. Consequently, in Figure 2a and Figure 2b the accumulated flow curves in the simulations are consistently reproduced although the final values are a bit higher. Concerning the comparison between the ATLAS and LSTF results in Figure 2c, it is shown that the coolant discharge in both facilities follows a similar trend and the final amount is alike.

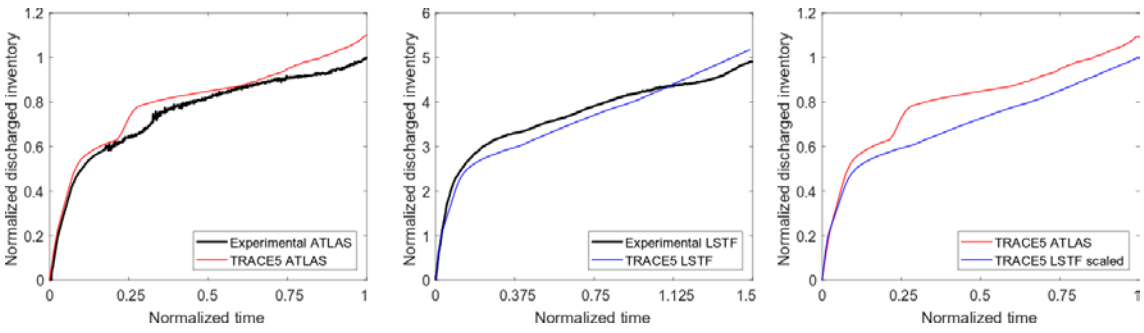

Figure 2: Accumulated discharged flow throw the break. a) ATLAS b) LSTF c) ATLAS and scaled LSTF

As Figure 3 depicts, the primary pressure falls sharply due to the loss of liquid during the first seconds. As the inventory through the break changes to two-phase flow, and then to gas flow, the depressurization is smoothed temporarily due to the MSIVs closure and then starts again to decrease. That trend continues until almost complete depressurization. The mass flow discharge and the primary pressure are directly related. Thus, the adjustment of the discharged inventory by means of choke flow multipliers is necessary for the simulations to avoid a sudden depressurization. As can be seen in Figure 3a and Figure 3b, the simulations provide pressure data very close to the experimental values. Moreover, Figure 3c shows good agreement between the ATLAS and LSTF pressure evolution, which justifies making a quantitative analysis of the quality of the scaling and its distortion.

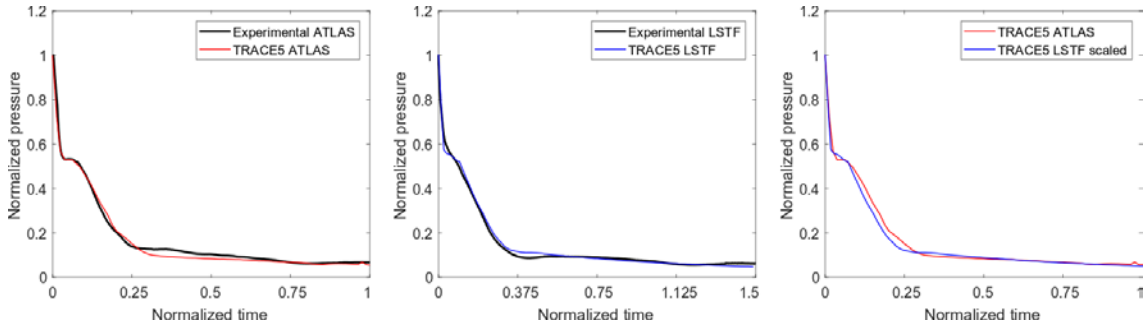

Figure 3: Primary pressure. a) ATLAS b) LSTF c) ATLAS and scaled LSTF

Together with the initial depressurization, the collapsed liquid level in the vessels falls rapidly and the HPI system actuates. From this moment, the PCT responses differ qualitatively between facilities, as Figure 4 indicates. In ATLAS (Figure 4a), the core dry out takes place soon. At this point, the core power is still high and the water that remains in the vessel is not enough to cool the heaters simulating the fuel. Therefore, a sudden and large increase in the peak cladding temperature (PCT) is produced. In this facility, the HPIS injection is not enough to recover the core level and the PCT does not decrease until the discharge of the accumulators. In LSTF, the HPIS injection is at first adequate to mitigate the core uncover and the dryout effects. However, due to the continuous boiling in the core and loss of coolant, another dryout occurs shortly before the injection of the accumulators. As a result, the PCT in LSTF (Figure 4b) presents two small peaks. In Figure 4c the two PCTs overlap. As a hypothesis to justify their obvious differences, the geometric aspects of the facilities and their subsequent effects are mainly postulated. In LSTF the upper plenum plate is closed and the only flow path between the upper plenum and the upper head are the control rod guide tubes. By contrast, the upper core plate in ATLAS is perforated. This would alter the liquid and gas mass flows between volumes in the vessels, which results in a different distribution of inventory in the primary system. In addition, the size of the hot legs affects the countercurrent flow phenomenon and the quantity of condensed liquid that returns to the vessel from the hot legs, and contributes to refill the core.

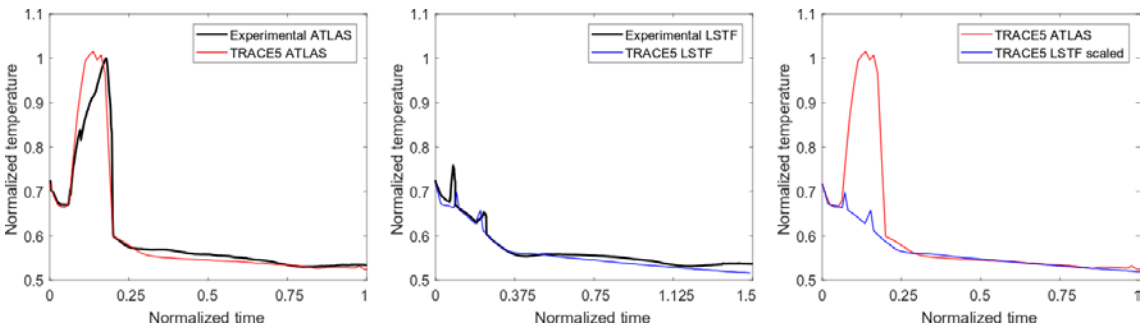

Figure 4: Peak cladding temperature. a) ATLAS b) LSTF c) ATLAS and scaled LSTF

Figure 5 shows the comparison of the ECCS injections between ATLAS and LSTF. The target mass flows of the HPIS and the LPIS in ATLAS are scaled down from the IB-CL-05 experiment, and then, equally divided into the two cold legs of the intact loop. Likewise, the initial inventory in the accumulators is also scaled from the LSTF conditions. Moreover, the injection rates depend on the pressure of the primary system. The HPIS and the LPIS are activated at the set points P_{HPI} and P_{LPI} and from then the flow rates are controlled by the speed of the safety injection pumps. Since the depressurization in both facilities presents very similar behavior, the time of activation of these ECCS is simultaneous and the evolution of the flow rates is equivalent (Figure 5a and Figure 5c). Figure 5b presents the injection of water from the accumulators. This management accident measure is able to bring the facilities to stable conditions due to a large amount of cold water that enters the systems. When the set point of action of the accumulators (P_{ACC}) is reached, their isolation valves are opened and their content is discharged by gravity as the primary systems are depressurized. As it is shown, the simulations do not reproduce the same trend for the mass flow. In ATLAS, the coolant is introduced roughly continuously but in LSTF two stages are distinguished and the injection is prolonged. Despite this fact, since the valves aperture and the discharge occur on time and the injected quantity of water is preserved, the behavior of other parameters like the pressures or temperatures are not altered.

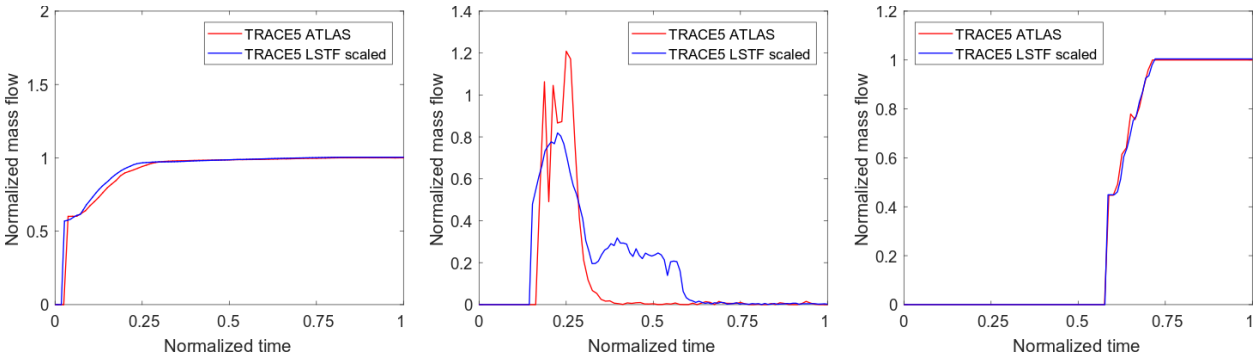

Figure 5: Safety system injections in ATLAS and scaled LSTF. a) HPI b) Accumulators c) LPI

4. SCALING ANALYSIS ASSESSMENT

4.1 Phases of the 13% IBLOCA experiment

The IBLOCA accidents may follow different evolution depending on the break size and location. Thus, according to the characteristics of the break, the sequence of events resembles more to those during a small or a large break. The main difference in the progress of these accidents lies in the occurrence or not of a period of time in which the primary pressure presents a plateau after the blowdown. This effect is produced when the pressure loss rate due to the loss of coolant and the heat transfer to the secondary system is compensated by the high production of steam in the core.

The first step in the scaling analysis is the division of the transients into phases to identify the dominant phenomena in each period and rank their importance. The partition into chronological phases and the duration of each phase are based on phenomenological considerations. Figure 6 shows a scheme of the partition of an IBLOCA according to the pressure evolution of the primary system. In this work, the limits that determine the beginning and end of each phase of the 13% IBLOCA rely on the experimental results of the A5.2 Test of the OECD-ATLAS project.

• Blowdown phase. The LOCA experiments start with the opening of a valve that simulates a break and, due to the high pressure and temperature conditions, a large amount of coolant begins to be discharged. As a consequence, the primary system rapidly depressurizes and, when the pressure falls below P_{SCRAM}, a SCRAM signal trips the power decay and the coast down of the pumps, closes the main steam isolation valves and stops the water supply to the steam generators. During the blowdown, the coolant in the primary system remains in liquid phase except for the pressurizer. This phase is completed when steam starts to form in the hot legs and in the vicinity of the break.

• Natural circulation phase. When the pumps stop, the circulation of coolant within the loops is owing to natural convection, that is, the fluid transport that arises because of the density difference between the heat source (core) and the heat sink (U-tubes). As a result of this phenomenon, two different regions are established along the loops. On one side, the core, upper plenum, hot legs and the upflow-side of the U-tubes comprise a two-phase region. On the other side, the downflow-side of the U-tubes where the coolant condenses, the loop seals, cold legs and the vessel downcomer comprise the liquid region. The natural circulation phase is held while the steam generators are still capable to remove the decay heat from the core. Another characteristic of this phase is the quasi-equilibrium condition of the pressure. Due to the evaporation rate in the vessel is large, the pressure gained compensates the loss of pressure produced by the discharge of coolant, the heat transfer to the secondary system and the heat losses.

• High-quality discharge. The size and location of the break used in the A5.2 Test produce a large loss of coolant and the rapid emptying of the system. Therefore, very high-quality mixture or steam are discharged soon through the break, and the pressure decreases again. As the primary pressure drives the HPI injection, the HPI mass flow increases and this has a double effect. The cold water favors the steam condensation and contributes to depressurize the primary system. Moreover, the increase of the HPI mass flow rate slightly increases the primary inventory, however, this amount of liquid is not enough to bring the facility to stable conditions. The phase finishes when the primary pressure is low enough to enable the action of the accumulators.

• Refill. The progressive depressurization of the primary system activates other emergency core cooling systems (ECCS). First, the accumulators discharge and most of the water levels are recovered. The injection of cold water into the downcomer results in condensation and the continuous decrease in primary pressure. At the LPI set point, its injection contributes to the vessel refilling. The transient finishes when the core is completely reflooded and the system stabilizes at very low pressure.

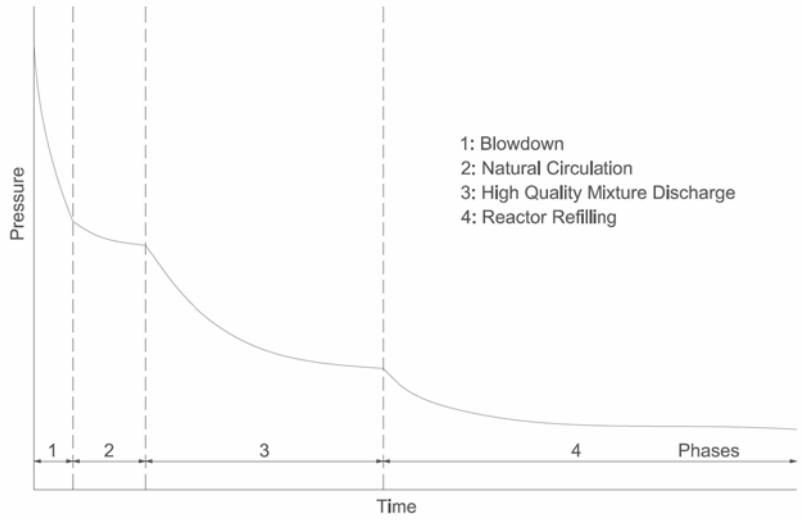

Figure 6: Primary pressure scheme for the IBLOCA transient.

4.2 Scaling of the blowdown phase

The blowdown phase initiates with the aperture of the break and the discharge of a large amount of coolant. This makes the primary system depressurization the dominant phenomenon during the phase.

Under the steady-state conditions at the beginning of the experiment, the primary system contains non-saturated water except for the pressurizer, which includes water and gas in saturation state. This condition is maintained during the entire phase until the pressurizer empties. Then, the whole system is simplified to a large volume of subcooled water consisting of the pressure vessel and the loops, to which a tank of saturated liquid and steam (the pressurizer) is connected.

The evolution of the pressure and the liquid level in the pressurizer during this phase are analyzed by evaluating the continuity equations for mass and energy. The mass balance supposes the mass flow leaving the pressurizer equal to the discharged flow through the break. Regarding the energy balance, the core and the pressurizer heaters are heat sources to the system, while the heat transfer to the secondary system and the heat losses are the heat sinks. [33]Muñoz-Cobo et al. (2018) details the mathematical development for the time-dependent level and pressure expressions in Eqs. (1) and (2). To achieve these equations, thermodynamic equilibrium is assumed between liquid and gas phases.

$$\frac{dL}{dt} = \frac{-\dot{m}_{prz} H_0}{V_{prz}(\rho_l - \rho_g)} - \frac{(H_0 - L)}{(\rho_l - \rho_g)} \cdot \frac{d\rho_g}{dp}\bigg|_{sat} \frac{dp}{dt} \quad (1)$$

$$\frac{dp}{dt} = \left(\frac{\partial p}{\partial \mu}\right)_v \frac{1}{M}\left[-\dot{m}_{prz}\left(h_{out} - \mu + \frac{\mu_{lg}}{v_{lg}}\right) + \dot{q}_{prz}\right] \quad (2)$$

Next, the equations are non-dimensionalized to compare the relative importance of the transfer processes considered by each term. For that, the following dimensionless magnitudes in Eq. (3) are defined by using reference parameters for each one of the phases of the transient.

(3)

$$p^* = \frac{p}{\Delta P_0} \qquad L^* = \frac{L}{H_0} \qquad t^* = \frac{t}{\tau_0} \qquad \dot{m}^* = \frac{\dot{m}}{\dot{m}_0}$$

$$\rho^* = \frac{\rho}{\rho_0} \qquad h^* = \frac{h}{h_0} \qquad v^* = \frac{v}{v_0} \qquad \dot{q}^* = \frac{\dot{q}}{\dot{q}_0}$$

$$\mu^* = \frac{\mu}{\mu_0} \qquad t^* = \frac{t}{\tau_0} \qquad \left(\frac{\partial \mu}{\partial p}\right)_v^* = \frac{\left(\frac{\partial \mu}{\partial p}\right)_v}{\left(\frac{\partial \mu}{\partial p}\right)_{v,0}} \qquad \left(\frac{\partial \rho_g}{\partial p}\right)_{sat}^* = \frac{\left(\frac{\partial \rho_g}{\partial p}\right)_{sat}}{\left(\frac{\partial \rho_g}{\partial p}\right)_{sat,0}}$$

Additionally, the characteristic time for each phase is defined by Eq. (4) as:

$$\tau_0 = M_0/\dot{m}_0 \quad (4)$$

For the blowdown phase, M_0 is the initial mass in the pressurizer and m_0 is the mean mass flow rate through the break during the period. The other reference thermal-hydraulic parameters are those of the starting point, since it is considered the most representative of the phase.

By substituting the non-dimensional magnitudes in the pressure and level equations (Eqs. (1) and (2)), the non-dimensional equations Eqs. (5) and (6) yield the π-monomial groups.

$$\frac{dL^*}{dt^*} = -\Xi_{\dot{L},\dot{m}} \frac{\dot{m}^*_{prz}}{(\rho_l - \rho_g)^*} - \Xi_{\dot{L},\dot{p}} \left(\frac{1-L^*}{\rho^*_f - \rho^*_g}\right) \left(\frac{d\rho_g}{dP}\right)^*_{sat} \left(\frac{dP}{dt}\right)^* \quad (5)$$

$$\frac{dp^*}{dt^*} = -\Xi_{\dot{p},\dot{m}\Delta h_{out}} \left(\frac{\partial p}{\partial \mu}\right)^*_v \frac{1}{M^*} \left[\dot{m}_{prz}{}^* (h_{out} - \mu)^*\right] - \Xi_{\dot{p},\dot{m}v} \left(\frac{\partial p}{\partial \mu}\right)^*_v \frac{1}{M^*} \dot{m}_{prz}{}^* v^* \frac{\mu_{lg}}{v_{lg}} + \Xi_{\dot{p},\dot{q}} \left(\frac{\partial p}{\partial \mu}\right)^*_v \frac{1}{M^*} \dot{q}^*_{prz} \quad (6)$$

Where the π-monomial groups are as shown in Table IV.
For ATLAS and LSTF, the groups are computed to calculate the ratios that determine the importance of each thermal-hydraulic process and to quantify the distortion between facilities. In Table IV, the values of the π-monomial groups during the blowdown are evaluated and compared. The first column lists the π-monomial groups, the second and fourth column shows their values for ATLAS and LSTF, respectively, and the third and fifth their importance. The distortion ratios between facilities are presented in the sixth column.

Table IV: Summary of the scaling approach results for the blowdown phase.

π-monomial groups	ATLAS groups	ATLAS importance	LSTF groups	LSTF importance	Distortion ratio
$\Xi_{\dot{L},\dot{m}} = \frac{\dot{m}_0}{M_0}\tau_0$	1	1	1	1	1
$\Xi_{\dot{L},\dot{p}} = \frac{\Delta P_0}{\rho_0}\left(\frac{d\rho_g}{dP}\right)_{sat,0}$	0.925	0.925	0.920	0.925	0.995
$\Xi_{\dot{p},\dot{m}\Delta h_{out}} = \frac{\tau_0}{\Delta P_0}\left(\frac{\partial p}{\partial \mu}\right)_{v,0} \frac{1}{M_0}\dot{m}_0(h_{out,0} - \mu_0)$	0.129	0.0972	0.131	0.0939	1.012
$\Xi_{\dot{p},\dot{m}v} = \frac{\tau_0}{\Delta P_0}\left(\frac{\partial p}{\partial \mu}\right)_{v,0} \frac{1}{M_0}\dot{m}_0 v_0 \frac{\mu_{lg,0}}{v_{lg,0}}$	1.4	1	1.4	1	0.999
$\Xi_{\dot{p},\dot{q}} = \frac{\tau_0}{\Delta P_0}\left(\frac{\partial p}{\partial \mu}\right)_{v,0} \frac{1}{M_0}\dot{q}_{prz,0}$	0.0108	0.00772	0.0149	0.0107	1.382

In regard of the π-monomial groups that govern the level variation, $\Xi_{\dot{L},\dot{m}}$ and $\Xi_{\dot{L},\dot{p}}$ have similar values in both facilities. Therefore, their ratios close to 1 indicate that the importance of one does not override the other. By contrast, the π-monomial group $\Xi_{\dot{p},\dot{m}v}$ in the depressurization rate equation is more than one order of magnitude higher than $\Xi_{\dot{p},\dot{m}\Delta h_{out}}$ and $\Xi_{\dot{p},\dot{q}}$. Based on the physical meaning of the dominant group, this implies that the change in specific volume governs the depressurization.

Regarding the phenomena distortion between both facilities, all the ratios are close to 1 as shown in Table IV. The group that gives the contribution of the net heat to depressurization, $\Xi_{\dot{p},\dot{q}}$, presents the greatest distortion. This is due to the scaling of the power supplied by the core and the pressurizer heaters are not preserved because both powers are not directly scaled, and they are modified to compensate the heat losses. However, this π-monomial group has the lowest importance and consequently, its distortion does not affect significantly the depressurization.

4.3 Scaling of the natural circulation phase

The natural circulation phase consists in the period in which the mass flow is driven by the balance between driving forces (gravity forces along SG downward side) and resisting forces (wall friction and local friction). During the phase, the inventory is continuous boiling in the core and the pressure gained almost compensates the loss of pressure produced by the loss of coolant and the heat transferred to the steam generators. Thus, the pressure in the primary system remains nearly constant and slightly higher than that in the secondary system. At one point, the mass flow rate in the top of the U-tubes region becomes one-phase gas and, due to the weakness of the gravity forces, natural circulation interrupts.

On account of the complexity that the analytical study of this phase could achieve, the real problem is simplified by making some assumptions. First, the control volume that is used is the entire primary system, and second, all the coolant is assumed to be a one field of two-phase mixture at saturation conditions. In this way, complex evaporation and condensation terms are eliminated from the mass and energy conservation equations, and the equations for the mass and pressure evolution result as follows:

$$\frac{dM}{dt} = \dot{m}_{HPIS} - \dot{m}_{break} \quad (7)$$

$$\frac{dp}{dt} = \frac{\left(\frac{\delta p}{\delta \mu_m}\right)_{v_m}}{M}\{\dot{m}_{HPIS}(h_l - \mu_m) - \dot{m}_{break}(h_m - \mu_m) + \dot{q}_{core} - \dot{q}_{SG} - \dot{q}_{loss}\} - \frac{\left(\frac{\delta p}{\delta v_m}\right)_{\mu_m}}{M\rho_m}(\dot{m}_{HPIS} - \dot{m}_{break}) \quad (8)$$

To carry out the non-dimensionalization process, the reference parameters are taken at the mean time of the natural circulation phase. By substituting the non-dimensional magnitudes in the pressure and level equations (Eqs. (7) and (8)), the non-dimensional equations Eqs. (9) and (10) yield the π-monomial groups.

$$\frac{dM^*}{dt^*} = \Xi_{\dot{M},\dot{m}}(\dot{m}^*_{HPIS} - \dot{m}^*_{break}) \quad (9)$$

$$\frac{dp^*}{dt} = \Xi_{\dot{p},\dot{m}(h_{in}-\mu_m)}\frac{\left(\frac{\delta p}{\delta \mu_m}\right)^*_{v_m}}{M^*}\dot{m}^*_{HPIS}(h^*_l - \mu^*_m) - \Xi_{\dot{p},\dot{m}(h_{out}-\mu_m)}\frac{\left(\frac{\delta p}{\delta \mu_m}\right)^*_{v_m}}{M^*}\dot{m}^*_{break}(h^*_m - \mu^*_m) + \Xi_{\dot{p},\dot{q}_{net}}\frac{\left(\frac{\delta p}{\delta \mu_m}\right)^*_{v_m}}{M^*}\dot{q}^*_{net} - \Xi_{\dot{p},\dot{m}v_m}\frac{\left(\frac{\delta p}{\delta v_m}\right)^*_{\mu_m}}{M^*}\frac{1}{\rho^*_m}(\dot{m}^*_{HPIS} - \dot{m}^*_{break}) \quad (10)$$

Table V displays the π-monomial groups and their importance for the natural circulation phase as was done for the previous phase.

Table V: Summary of the scaling approach results for the natural circulation phase

π-monomial groups	ATLAS groups	ATLAS importance	LSTF groups	LSTF importance	Distortion ratio
$\Xi_{\dot{M},\dot{m}} = \frac{\dot{m}_0}{M_0}\tau_0$	1	1	1	1	1
$\Xi_{\dot{p},\dot{m}(h_{in}-\mu_m)} = \frac{\tau_0}{\Delta P_0}\frac{\left(\frac{\delta p}{\delta \mu_m}\right)_{v_m,0}}{M_0}\dot{m}_0\left(h_{in,0}-\mu_{m,0}\right)$	-0.456	0.09	-0.498	0.078	0.915
$\Xi_{\dot{p},\dot{m}(h_{out}-\mu_m)} = \frac{\tau_0}{\Delta p_0}\frac{\left(\frac{\delta p}{\delta \mu_m}\right)_{v_m,0}}{M_0}\dot{m}_0\left(h_{out,0}-\mu_{m,0}\right)$	-0.636	0.128	-0.692	0.109	0.919
$\Xi_{\dot{p},\dot{q}_{net}} = \frac{\tau_0}{\Delta P_0}\frac{\left(\frac{\delta p}{\delta \mu_m}\right)_{v_m,0}}{M_0}\dot{q}_0$	4.962	1	6.34	1	0.782
$\Xi_{\dot{p},\dot{m}v_m} = \frac{\tau_0}{\Delta P_0}\frac{\left(\frac{\delta p}{\delta v_m}\right)_{\mu_m,0}}{M_0\rho_{m,0}}\dot{m}_0$	4.92	0.991	4.91	0.77	1.002

The π-monomial group that relates the balance of the mass flow rates entering and leaving the system and its contribution to the total mass of the system, $\Xi_{\dot{M},\dot{m}}$, is equal to 1 by definition. Regarding the π-monomial groups derived from the pressure evolution, the net enthalpy of these flow rates, $\Xi_{\dot{p},\dot{m}(h_{in}-\mu_m)}$ and $\Xi_{\dot{p},\dot{m}(h_{out}-\mu_m)}$, is not relevant to the depressurization if compared to the other groups. As expected and the group $\Xi_{\dot{p},\dot{q}_{net}}$ shows, the net heat transfer to the system is the most important phenomenon during this phase for being a natural circulation driver.

All the ratios giving the distortion are in the range to consider the phenomena well scaled ([35]Wulff, 1996). It is noticeable that the greatest distortion becomes from the net heat transfer to the system in spite of its importance. This is due to the scaling of the core power and the differences in heat losses effect between ATLAS and LSTF.

4.4 Scaling of the high-quality discharge phase

After a brief natural circulation phase, the circulation interrupts suddenly and the inventory is distributed along the loops in three regions depending on the fluid conditions, i.e., steam, liquid and two-phase mixture. The steam generator U-tubes, the upper head and top of the upper plenum regions and the upper part of the hot legs comprise the steam field. The lower part of the hot legs and the core contain a two-phase mixture. The lower plenum, the downcomer, the loop seals and the cold legs, which contain the liquid field, constitute the third region. According to this distribution of water, very high quality or pure steam flow is discharged through the break. Due to this, the pressure in the primary system decreases constantly until the ending of the phase, when the accumulators start to inject cold water.

Throughout this phase, the scaling analysis is developed by considering the primary system as a unique control volume divided into three regions, in which only the mass and energy balances change. The equation (11) and (12) model the inventory and pressure evolution ([33]Muñoz-Cobo, 2018), where the terms coming from the inter-filed exchange can be neglected, as proven by [32]Banerjee, 1997.

$$\frac{dM_{RCS}}{dt} = \frac{d}{dt}\sum_{k=l,m,g}\rho_k V_k = \dot{m}_{HPI} - \dot{m}_{break} \quad (11)$$

$$\frac{dp}{dt} = \frac{1}{\sum_{k=l,m,g}\frac{\rho_k V_k}{\left(\frac{\partial p}{\partial v_k}\right)_{\mu_k}}} \cdot \left[\sum_{k=l,m,g}\frac{\left(\frac{\partial p}{\partial \mu_k}\right)_{v_k}}{\left(\frac{\partial p}{\partial v_k}\right)_{\mu_k}}\left[\sum \dot{m}_{in,k}\left(h_{in,k}-\mu_k\right) - \sum \dot{m}_{out,k}\left(h_{out,k}-\mu_k\right) + \dot{q}_{net,k}\right] - \sum_{k=l,m,g} v_k\left[\dot{m}_{in,k} - \dot{m}_{out,k}\right]\right] \quad (12)$$

The following variables, $C_{1,k}$ and C_2, and their respective non-dimensional variables, $C_{1,k}$ and C_2, are defined to simplify the expression for the pressure evolution (Eq. (12)) and its normalization ([33]Muñoz-Cobo (2018)).

$$C_{1,k} = \frac{\left(\frac{\partial p}{\partial \mu_k}\right)_{v_k} \Big/ \left(\frac{\partial p}{\partial v_k}\right)_{\mu_k}}{\sum_{k\prime=l,m,g}\frac{\rho_{k\prime}V_{k\prime}}{\left(\frac{\partial p}{\partial v_{k\prime}}\right)_{\mu_{k\prime}}}} \quad (13)$$

$$C_2 = \frac{1}{\sum_{k\prime=l,m,g}\frac{\rho_{k\prime}V_{k\prime}}{\left(\frac{\partial p}{\partial v_{k\prime}}\right)_{\mu_{k\prime}}}} \quad (14)$$

$$C_{1,k}^* = \frac{C_{1,k}}{C_{1,k,0}} \quad (15)$$

$$C_2^* = \frac{C_2}{C_{2,0}} \quad (16)$$

By substituting the non-dimensional magnitudes defined in Eqs. (15) and (16), in the mass and pressure equations, the non-dimensional expressions Eqs. (17) and (18) yield the π-monomial groups for the phase.

$$\frac{dM^*}{dt^*} = \Xi_{\dot{M},\dot{m}}\sum_{k=l,m,g}\left[\sum \dot{m}_{in,k}^* - \sum \dot{m}_{out,k}^*\right] \quad (17)$$

$$\frac{dp^*}{dt} = \sum_{k=l,m,g}\Xi_{\dot{p},\dot{m}(h_{in}-\mu)k}\cdot C_{1,k}^*\sum \dot{m}_{in,k}^*\left(h_{in,k}-\mu_k\right)^* - \sum_{k=l,m,g}\Xi_{\dot{p},\dot{m}(h_{out}-\mu)k}\cdot C_{1,k}^*\sum \dot{m}_{out,k}^*\left(h_{out,k}-\mu_k\right)^* + \sum_{k=l,m,g}\Xi_{\dot{p},\dot{q}_{net,k}}\cdot C_{1,k}^*\dot{q}_{net,k}^* - \sum_{k=l,m,g}\Xi_{\dot{p},\dot{m}v_k}\cdot C_2^* v_k^*\left[\sum \dot{m}_{in,k}^* - \sum \dot{m}_{out,k}^*\right] \quad (18)$$

Table VI presents the dimensionless groups related to the mass and pressure evolution during the high-quality discharge phase, together with their importance in the discharge of inventory and the depressurization processes. Furthermore, the last column of Table VI shows the scaling distortion between ATLAS and LSTF through the ratio of the π-monomial groups of both facilities.

Table VI: Summary of the scaling approach results for the high quality discharge phase.

π-monomial groups	ATLAS groups	ATLAS importance	LSTF groups	LSTF importance	Distortion ratio
$\Xi_{\dot{M},\dot{m}} = \frac{\dot{m}_0}{M_0}\tau_0$	1.000	1.000	1.000	1.000	1.000
$\Xi_{\dot{p},\dot{m}(h_{in}-\mu)l} = \frac{\tau_0}{\Delta P_0} C_{1,l,0}\dot{m}_0\left(h_{in,l,0} - \mu_{l,0}\right)$	0.201	0.004	0.248	0.0004	0.813
$\Xi_{\dot{p},\dot{m}(h_{in}-\mu)m} = \frac{\tau_0}{\Delta P_0} C_{1,m,0}\dot{m}_0\left(h_{in,m,0} - \mu_{m,0}\right)$	-4.04	0.081	-4.54	0.0805	0.885
$\Xi_{\dot{p},\dot{m}(h_{in}-\mu)g} = \frac{\tau_0}{\Delta P_0} C_{1,g,0}\dot{m}_0\left(h_{in,g,0} - \mu_{g,0}\right)$	49.852	1.000	56.41	1	0.883
$\Xi_{\dot{p},\dot{m}(h_{out}-\mu)l} = \frac{\tau_0}{\Delta P_0} C_{1,l,0}\dot{m}_0\left(h_{out,l,0} - \mu_{l,0}\right)$	0.232	0.0046	0.285	0.00494	0.814
$\Xi_{\dot{p},\dot{m}(h_{out}-\mu)m} = \frac{\tau_0}{\Delta P_0} C_{1,m,0}\dot{m}_0\left(h_{out,m,0} - \mu_{m,0}\right)$	0.128	0.0025	0.121	0.00215	1.055
$\Xi_{\dot{p},\dot{m}(h_{out}-\mu)g} = \frac{\tau_0}{\Delta P_0} C_{1,g,0}\dot{m}_0\left(h_{out,g,0} - \mu_{g,0}\right)$	49.852	1.000	56.41	1.000	0.883
$\Xi_{\dot{p},\dot{q}_{net,l}} = \frac{\tau_0}{\Delta P_0} C_{1,l,0}\dot{q}_{net,l,0}$	0.108	0.0022	0.103	0.0018	1.041
$\Xi_{\dot{p},\dot{q}_{net,m}} = \frac{\tau_0}{\Delta P_0} C_{1,m,0}\dot{q}_{net,m,0}$	-1.52	0.0304	-1.41	0.025	1.077
$\Xi_{\dot{p},\dot{q}_{net,g}} = \frac{\tau_0}{\Delta P_0} C_{1,g,0}\dot{q}_{net,g,0}$	10.9	0.219	9.78	0.174	1.118
$\Xi_{\dot{p},\dot{m}v_l} = \frac{1}{\sum_k \frac{M_k}{\left(\frac{\partial p}{\partial v_k}\right)_{\mu_k}}} \frac{\tau_0}{\Delta P_0}\dot{m}_0 v_{l,0}$	-0.164	0.0033	-0.2	0.00355	0.819
$\Xi_{\dot{p},\dot{m}v_m} = \frac{1}{\sum_k \frac{M_k}{\left(\frac{\partial p}{\partial v_k}\right)_{\mu_k}}} \frac{\tau_0}{\Delta P_0}\dot{m}_0 v_{m,0}$	-0.939	0.0188	-0.887	0.0157	1.058
$\Xi_{\dot{p},\dot{m}v_g} = \frac{1}{\sum_k \frac{M_k}{\left(\frac{\partial p}{\partial v_k}\right)_{\mu_k}}} \frac{\tau_0}{\Delta P_0}\dot{m}_0 v_{g,0}$	-3.82	0.0766	-4.45	0.0789	0.858

As in the previous phases, the group related to the contribution of the balance of mass flow rates to the total inventory of the system, $\Xi_{\dot{M},\dot{m}}$, is equal to 1. Each one of the groups belonging to the depressurization process has three values, each one of them associated with one field (liquid, mixture or gas). For all the groups, the gas phase terms are those of major contribution. In fact, in terms of importance, the net energy entering and leaving the system, $\Xi_{\dot{p},\dot{m}(h_{in}-\mu)g}$ and $\Xi_{\dot{p},\dot{m}(h_{out}-\mu)g}$, are the most important terms followed by $\Xi_{\dot{p},\dot{q}_{net,g}}$.

Regarding the ratios between the groups, all the values are between 0.813 and 1.118, so it follows that there is no significant distortion.

4.5 Scaling of the refill phase

The refilling phase is characterized by the operation of the core cooling systems, which inject a large amount of water into the system until the core is completely reflooded. The phase starts when the pressure has decreased until the accumulators set point. The accumulators discharge sub-cooled water that enters the system through the cold legs. In this way, the liquid levels in the core and the loop seals are rapidly recovered. This is also favored by the steam condensation, which diminishes the pressure and allows the increase of the HPI mass flow rate and the LPI actuation. Furthermore, the refill of the system significantly reduces the vapor quality at the break and the pressure stabilizes.

For this phase, the control volume divided into three fields and the equations for the mass and pressure evolution are the same ones than in the high-quality discharge phase. Consequently, the π-monomial groups in Table VII are the same as well, despite their values and the comparison result different.

Table VII: Summary of the scaling approach results for the refilling phase.

π-monomial groups	ATLAS groups	ATLAS importance	LSTF groups	LSTF importance	Distortion ratio
$\Xi_{\dot{M},\dot{m}}$	1.000	1.000	1.000	1.000	1.000
$\Xi_{\dot{p},\dot{m}(h_{in}-\mu)l}$	0.225	0.00014	0.315	0.00014	0.714
$\Xi_{\dot{p},\dot{m}(h_{in}-\mu)m}$	-13.7	0.0086	-19.1	0.0084	0.715
$\Xi_{\dot{p},\dot{m}(h_{in}-\mu)g}$	936.49	0.59	1241.6	0.547	0.754
$\Xi_{\dot{p},\dot{m}(h_{out}-\mu)l}$	0.282	0.00017	0.394	0.00017	0.716
$\Xi_{\dot{p},\dot{m}(h_{out}-\mu)m}$	0.283	0.00017	0.377	0.00016	0.751
$\Xi_{\dot{p},\dot{m}(h_{out}-\mu)g}$	936.49	0.59	1241.6	0.547	0.754
$\Xi_{\dot{p},\dot{q}_{net,l}}$	-1.57	0.00098	-2.34	0.001	0.671
$\Xi_{\dot{p},\dot{q}_{net,m}}$	62.9	0.0396	95	0.0418	0.662
$\Xi_{\dot{p},\dot{q}_{net,g}}$	-1590	1	-2270	1	0.698
$\Xi_{\dot{p},\dot{m}v_l}$	-0.171	0.00012	-0.249	0.00011	0.686
$\Xi_{\dot{p},\dot{m}v_m}$	-2.55	0.00161	-3.39	0.00149	0.753
$\Xi_{\dot{p},\dot{m}v_g}$	-26	0.0164	-36.2	0.0159	0.7177

Table VII displays the ranking of importance of the π-monomial groups that govern the evolution of mass and pressure during the refilling phase. The value and importance of the group derived from the mass conservation equation, $\Xi_{\dot{M},\dot{m}}$, is 1 again by definition. Concerning the groups related to the pressure evolution, the gas phase terms are those of major contribution as occurring in the previous phase. However, in this phase, the most important term is that of the net heat transfer, $\Xi_{\dot{p},\dot{q}_{net,g}}$, followed by the ones about the enthalpy of the incoming and outgoing flow rates.

Even though the refilling is the phase that presents the most distortion, the analysis shows good scalability since all the ratios between ATLAS and LSTF are equal or lower to 1 and higher than 0.5.

5 CONCLUSIONS

This work is intended to analyze a 13% IBLOCA counterpart test between ATLAS and LSTF facilities. To that end, experimental results of the tests A5.2 and IB-CL-05 belonging to OECD-ATLAS and OECD/NEA ROSA-2 projects, respectively, are compared and simulated with TRACE5 code. The experiments in question represent a Double-Ended Guillotine Break (DEGB) of one of the emergency cooling system (ECCS) piping nozzle connected to a cold leg. Under these conditions, full injection of the emergency cooling system and total failure of auxiliary feedwater were assumed as the management accident measures. Moreover, the first approach of the top-down scaling methodology is applied to the simulation results to assess the scaling methodology between facilities. Major results of the work are summarized as follows:

1. Two TRACE5 models of the ATLAS and LSTF facilities have been set up and it has proved to be a suitable tool to simulate their behavior. Thus, the code predictions are in quite close agreement with the available experimental data. The most important phenomena, like primary system depressurization, break discharge or peak cladding temperature, have been correctly simulated.

2. The IBLOCA experiment begins with the opening of the break and, as a consequence, a large loss of coolant. Given these conditions, the HPIS injection together with the accumulators discharge could successfully recover the coolant inventory in the pressure vessel and quench the core; therefore, the ECCS proves to be an effective accident management measure.

3. Simulation data in ATLAS are presented together with the scaled data in the LSTF by making use of the global scaling ratios of length ($l_0 = 0.52$) and volume ($l_0 d_0^2 = 0.201$) and by applying the three-level scaling methodology to obtain other parameters. The comparison between ATLAS and LSTF data reveals that thermal-hydraulic phenomena and the overall sequence of major events are equivalent. This discloses the possibility to extrapolate some thermal-hydraulic variables between both facilities to predict phenomena under this type of scenario.

4. A dimensionless analysis is developed at the primary system level to the four chronological phases of the transient: Blowdown, natural circulation, high-quality discharge and refilling. The π-monomial groups derived from the equations that govern the depressurization and inventory discharge assess the similarity of the transfer processes (mass, enthalpy, heat and volumetric flow) for the four phases. Likewise, the net heat transfer to the primary system is identified as the main source of scaling distortion.

Acknowledgements

The authors are grateful to the Management Board of the OECD-ATLAS Project for their consent to this publication, and thank the Spanish Nuclear Regulatory Body (CSN) for the technical and financial support under the agreement STN/4524/2015/640. The authors also thank Prof. J.L. Munoz-Cobo for his advice and the willingness to share his insights on the scaling methodologies.

REFERENCES

1 Freixa, J., Belaid, S., Zerkak, O., 2013. Thermal-hydraulic system code performance for SBLOCA phenomenology under different geometries and scales. 15th International Topical Meeting on Nuclear Reactor Thermal Hydraulics (NURETH-15), Pisa, Italy, May 12-17, 2013. NURETH15-331.

2 Belaid, S., Freixa, J., Zerkak, O., 2010. Analysis of the Test OECD-PKL2 G7.1 with the Thermal-Hydraulic System Code TRACE. U.S. Nuclear Regulatory Commission, Washington, DC, NUREG/IA-0432.

3 Lafi, A. Y., Reyes Jr, J. N., 2000. Comparative study of station blackout test in APEX and ROSA/AP600. Nuclear Technology, 130, 177-183.

4 Park, H. S. et al., 2014. A counterpart test of the VISTA-ITL SB-SIS-07 using the FESTA (SMART-ITL) facility for the SMART design. Transactions of the Korean Nuclear Society Spring Meeting, Jeju, Korea, May 29-30, 2014.

5 Carlos, S. et al., 2016. Post-test analysis of the ROSA/LSTF and PKL counterpart test. Nuclear Engineering and Design, 297,81-94.

6 Park, Y., 2017.Test Report on the OECD-ATLAS A5.1 Test: Counterpart Test for LSTF 1% Cold-Leg Break LOCA (SB-CL-32). Korea Atomic Energy Research Institute, OECD-ATLAS-TR-07.

7 Yang, J., Choi, S.W., Lim, J., Lee, D. Y., Rassame, S., Hibiki, T., Ishii, M., 2013. Counterpart experimental study of ISP-42 PANDA tests on PUMA facility. Nuclear Engineering and Design, 258, 249-257.

8 Takeda, T., et al., 2012. RELAP5 Analyses of OECD/NEA ROSA-2 Project Experiments on Intermediate-Break LOCAs at Hot or Cold Leg. Journal of Power and Energy Systems, 6, 87-98.

9 D'Auria, F., 2017. Thermal-Hydraulics of Water Cooled Nuclear Reactors. Woodhead Publishing.

10 USNRC, 1998. Risk-Informed Changes to Loss-of-Coolant Accident Technical Requirements. The United States Nuclear Regulatory Commission, 10 CFR Technical Report, 70, 214.

11 Bajorek, S. M., Petkov, N., 2001. Realistic Small- and Intermediate-Break Loss-of-coolant Accident Analysis Using WCOBRA/TRAC. Nuclear Technology, 136, 50-62.

12 Addabbo, C., Annunziato, A., 2012. The LOBI Integral System Test Facility Experimental Programme. Science and Technology of Nuclear Installations, 2012, ID238019.

13 D'Auria, F., et al., 2000. SPES-99 IBLOCA analysis with the RELAP5 MOD 3.2 code. International Conference Nuclear Energy in Central Europe 2000. Bled, Slovenia, September 11-14, 2000.

14 Abe, S., Satou, A., Takeda, T., Nakamura, H., 2014. RELAP5 analyses of multi-dimensional flow in the core on the core cooling during LSTF cold-leg intermediate break LOCA experiments in the OECD/NEA ROSA-2 Project. Journal of Science and Technology, 51, 10, 1164-1176.

15 NEA/OECD, 2016. 2016 NEA Annual Report. NEA No. 7349.

16 Bestion, D., D'Dauria, F., Lien, P., Nakamura, H., 2017. A state-of-the-art report on scaling in system thermal-hydraulics applications to nuclear reactor safety and design. OECD, Nuclear Safety NEA/CSNI/R(2016)14.

17 Takeda, T., Ohtsu, I., 2017. RELAP5 uncertainty evaluation using ROSA/LSTF test data on PWR 17% cold leg intermediate-break LOCA with single-failure ECCS. Annals of Nuclear Energy, 109, 9–21.

18 KAERI, 2014. Scaling Analysis Report of the ATLAS Facility. Korea Atomic Energy Research Institute, KAERI/TR-5465/2014.

19 Choi, K.Y., Park, H.S., Euh, D.J., Kwon, T.S., Baek, W.P., 2017. Simulation capabilities of the ATLAS facility for major design-basis accidents. Nuclear Technology, 156:3, 256-269.

20 The ROSA-V Group, 2003. ROSA-V Large Scale Test Facility (LSTF) system description for the third and fourth simulated fuel assemblies. Japan Atomic Energy Agency (JAEA), Technical Report JAERI-Tech 2003-037.

21 Nakamura, H., et al., 2009. Overview of recent efforts through ROSA/LSTF experiments. Nuclear Engineering and Technology, 41 (6), 753–764.

22 USNRC, 2010. TRACE V5.0 USER'S MANUAL. In: Modeling Guidelines, vol. 2. U.S. Nuclear Regulatory Commission, Washington, DC.

23 Lorduy-Alós. M., Gallardo, S., Verdú, G., 2018. Simulation studies on natural circulation phenomena during an SBO accident. Applied Thermal Engineering, 139, 514-523.

24 Freixa, J., Martínez-Quiroga, V., Reventós, F., 2017. Modelling guidelines for CCFL representation during IBLOCA scenarios of PWR reactors. 17th International Topical Meeting on Nuclear Reactor Thermal Hydraulics (NURETH-17), Xi'an, China, September 3-8, 2017.

25 Kim, H. T., No, H. C., 2001. Assessment of RELAP5_MOD3.2.2y Against Flooding Database in Horizontal-to-Inclined Pipes. U.S. Nuclear Regulatory Commission, Washington, DC, NUREG_IA-0203.

26 Oussoren, A., Riznic, J., Revankar, S.T., 2017. Assessment of Critical Subcooled Flow Through Cracks in Largeand Small Pipes Using TRACE and RELAP5. U.S. Nuclear Regulatory Commission, Washington, DC, NUREG/IA-0457.

27 Zuber, N., 1991. Hierarchical Two-Tiered Scaling Analysis - Appendix D: An Integrated Structure and Scaling Methodology for Severe Accident Technical Issue Resolution. U.S. Nuclear Regulatory Commission, Washington, DC, NUREG/CR-5809.

28 Zuber, N., Wulff, W., Rohatgi, U.S., Catton, I., 2005. Application of fractional scaling analysis (FSA) to loss of coolant accidents (LOCA), Part 1: methodology development. 11th International Topical Meeting on Nuclear Reactor Thermal-Hydraulics (NURETH-11), Avignon, France.

29 Ishii, M., Kataoka, I., 1983. Similarity analysis and scaling criteria for LWR's under single-phase and two-phase natural circulation. Argonne National Laboratory, NUREG/CR-3267, ANL-83-32.

30 Ishii, M. et al., 1998. The Three Level Scaling Approach with Application to the Purdue University Multidimensional Integral Test Assembly (PUMA). Nuclear Engineering and Design, 186, 177-211.

31 Buckingham, E., 1914. On physically similar systems; illustrations of the use of dimensional equations. Phys. Rev. 4, 345–376.

32 Banerjee, S., Ortiz, M. G., Larson, T. K., Reeder, D. L., 1997. Top-Down Scaling Analyses. Methodology for AP600 Integral Tests, INEL-96/0040, May 1997.

33 Muñoz-Cobo, J. L., Berna, C., Escrivá, A., 2018. Top-down scaling methodology from the LSTF facility to a three loop PWR plant applied to a SBLOCA event – The ROSA 1.2 test. Nuclear Engineering and Design, 327, 248–273.

34 Wulff, W., Rohatgi, U., 1998. System Scaling for the Westinghouse AP600 Pressurized Water Reactor and Related Test Facilities. USNRC Report, Brookhaven National Laboratory, NUREG/CR-5541.

35 Wulff, W., 1996. Scaling of termohydraulic systems. Nuclear Engineering and Design, 163, 359–395.

36 Liao, J., 2016. System scaling analysis for modeling small break LOCA using the FULL SPECTRUM LOCA evaluation model. Annals of Nuclear Energy, 87, 443-453.

37 Bae, B. U., 2017.Test Report on the OECD-ATLAS A5.2 Test: Counterpart Test of Cold Leg Intermediate Break (13%) Loss-of-Coolant-Accident (IBLOCA) in ATLAS. Korea Atomic Energy Research Institute, OECD-ATLAS-TR-08.

38 Japan Atomic Energy Agency (JAEA), 2013. Final Data Report of ROSA-2/LSTF IB-CL-05 (Cold Leg Intermediate Break LOCA. JAEA, IB-CL-05.